Aerosol Science and Technology

ISSN: 0278-6826 (Print) 1521-7388 (Online) Journal homepage: http://www.tandfonline.com/loi/uast20

Fractal scaling of soot packing density across five size decades

Pai Liu, William R. Heinson & Rajan K. Chakrabarty

To cite this article: Pai Liu, William R. Heinson & Rajan K. Chakrabarty (2017) Fractal scaling of soot packing density across five size decades, Aerosol Science and Technology, 51:7, 879-886, DOI: 10.1080/02786826.2017.1316359

To link to this article: http://dx.doi.org/10.1080/02786826.2017.1316359

View supplementary material

Accepted author version posted online: 13 Apr 2017.
Published online: 13 Apr 2017.

Submit your article to this journal

Article views: 87

View related articles

View Crossmark data

Full Terms & Conditions of access and use can be found at
http://www.tandfonline.com/action/journalInformation?journalCode=uast20

Download by: [Washington University in St Louis] **Date:** 29 June 2017, At: 10:10

AEROSOL SCIENCE AND TECHNOLOGY
2017, VOL. 51, NO. 7, 879–886
https://doi.org/10.1080/02786826.2017.1316359

Taylor & Francis
Taylor & Francis Group

Check for updates

Fractal scaling of soot packing density across five size decades

Pai Liu*, William R. Heinson*, and Rajan K. Chakrabarty

Department of Energy, Environmental and Chemical Engineering, Washington University in St. Louis, St. Louis, Missouri, USA

ABSTRACT

We experimentally map the scaling laws for packing density (θ_f, solid component volume fraction) of soot aggregates across five orders of magnitude of size (R_g/a, normalized radius of gyration by monomer radius). The $\theta_f - R_g/a$ scaling relationship evolves through three successive regimes with distinct power-law exponents of -1.20 ± 0.01, -0.58 ± 0.06, and -1.31 ± 0.14. The first cross-over agrees with the classical aerosol-to-gel transition theory. This agreement, however, breaks down at the second cross-over point, where a late-stage cluster-cluster aggregation of aerosol gels takes over.

ARTICLE HISTORY
Received 10 January 2017
Accepted 23 March 2017

EDITOR
Matti Maricq

Introduction

Soot aggregates are produced from incomplete combustion of hydrocarbon fuels in a wide range of natural and anthropogenic systems, for example, vehicular engines, biomass burning, and wildfires (Chao et al. 1998; Park et al. 2004; Kumfer et al. 2006; Law 2010; Rehman et al. 2011; Chakrabarty et al. 2014a). These aggregates constitute of repeating near-spherical monomers, and are fractal-like and porous in their morphology and composition, respectively (Forrest and Witten 1979; Sorensen 2001, 2011). The packing density (θ_f)—defined as the fraction of the sub-volume taken by solid matter—is a fundamental property of these aggregates with many important implications. θ_f determines the transport characteristics and radiative forcing of these aggregates in the atmosphere (Bond et al. 2013; Chakrabarty et al. 2014a; Liu and Chakrabarty 2016; Heinson and Chakrabarty 2016). Accurate knowledge of θ_f is necessary to determine the extent of particle deposition in human lungs (Taulbee and Yu 1975; Hinds 1999). When it comes to synthesis of these aggregates for commercial purposes, a control of θ_f renders tailoring of desirable material properties, such as permeability, mechanical strength, thermal, and electrical conductivities (Johnson et al. 1996; Sánchez-González et al. 2005; Dhaubhadel et al. 2007; Greaves et al. 2011; Sakai et al. 2016).

Aggregate θ_f scales with radius of gyration (R_g) following a fractal power-law relationship,

$$\theta_f = k_f \left(R_g/a\right)^{D_f - 3}, \quad [1]$$

where k_f is the fractal prefactor, a is one monomer radius, and D_f is the mass fractal dimension that controls how fast θ_f decreases with increasing R_g (Forrest and Witten 1979; Sorensen 2001, 2011; Zangmeister et al. 2014). The value of D_f provides insight into the aggregate growth mechanism in a system. Aerosol aggregates with $R_g <$ 1 μm have been shown to grow via the diffusion-limited cluster-cluster aggregation (DLCA) mechanism with a characteristic $D_f \approx 1.78$ (Sorensen 2001, 2011). Beyond this size range, DLCA aggregates that are non-coalescent tend to behave as "super-monomers" and jam together to form percolated networks (hereafter percolates) with a $D_f \approx 2.5$ (Sorensen et al. 1998; Sorensen and Chakrabarti 2011). This percolation phenomenon of aerosol aggregates was first observed by Sorensen et al. (1998) and termed as aerosol gelation (Sorensen and Chakrabarti 2011). The theory of aerosol gelation is however not exhaustive to describe the growth of particles with large R_g. Multiple mechanisms have been suggested to take precedence successively in the growth regime $R_g >$ 1 μm (Kim et al. 2006). This implies a varying power-law exponent for θ_f in the large R_g/a limit, different from that predicted by the classical percolation model, ca. −0.5.

CONTACT Rajan K. Chakrabarty chakrabarty@wustl.edu Department of Energy, Environmental & Chemical Engineering, Washington University in St. Louis, One Brookings Drive, Campus Box 1180, St. Louis, MO 63130, USA.

Color versions of one or more of the figures in the article can be found online at www.tandfonline.com/uast.

Supplemental data for this article can be accessed on the publisher's website.

*These authors contributed equally to this work.

© 2017 American Association for Aerosol Research

There exist very limited studies on the experimental determination of θ_f for fractal aggregates with R_g/a reaching the large limit. Manley et al. (2004) showed aggregate structure tends to catastrophically break down when R_g/a reaches 10^3; thus the direct measurement of θ_f for the particles that are intact could be hindered by their mechanical instability. More recently, Zangmeister et al. (2014) reported the measurement of θ_f for rigid aggregates subjected to omnidirectional compaction forces. A remarkable scale-invariant $\theta_f \approx 0.36$ of the aggregates was observed for R_g/a across many orders of magnitude (Zangmeister et al. 2014). This confounding scale-independence, implying lack of any growth mechanism beyond percolation, has in part motivated this current study. Our objective herein is to provide a complete picture of the scaling relationship of θ_f across five orders of magnitude of R_g/a for freshly produced soot aggregates and infer their size delimited growth mechanism.

Methods

Sub-micron size aggregates

For soot aggregates with $R_g < 1$ μm, we deduced their θ_f based on previously published mass-mobility experimental data. Cross et al. (2010) had generated nascent soot aggregates using an ethylene flat flame burner and measured the mass (M) of these aggregates with certain mobility diameter (d_m) using a tandem differential mobility analyzer (DMA)—centrifugal particle mass analyzer (CPMA)—condensational particle counter (CPC) setup (Park et al. 2004; Cross et al. 2010; Zangmeister et al. 2014). We estimated N of these aggregates from the aggregate-to-monomer mass ratios. The monomer density ρ and average radius a were taken as 1812 kg/m^3 and 16 nm, respectively (Cross et al. 2010; see the online supplementary information (SI) S1). We estimated aggregate R_g from their d_m using the well-established empirical relationship for DLCA aggregates with $N < 100$ (Sorensen 2011):

$$\frac{d_m}{2R_g} = 1.29N^{-0.1}. \quad [2]$$

Finally, we calculated aggregate θ_f using the expression:

$$\theta_f = \frac{3M}{4\pi R_g^3 \rho}. \quad [3]$$

Super-micron size aggregates

Soot aggregates with $R_g > 1$ μm were generated using a novel buoyancy-opposed flame (BOF) reactor (Chakrabarty et al. 2012, 2014b; Liu et al. 2015) fueled by ethylene. Emitted particles were collected onto conducting carbon films (Ted Pella Inc., Redding, CA, USA) installed in a multistage size-segregated aerosol impactor (MPS-6, California Measurements Inc., Sierra Madre, CA, USA). Aggregate morphology was characterized using scanning electron microscope (SEM, Nova-230, FEI, Hillsboro, OR, USA) and custom-built image processing software. The number of monomers constituting an aggregate as seen in an image (N_{2d}) was estimated by the ratio of the aggregate's projected area (A_p) to the monomer cross-section area πa^2. N_{2d} was next converted to its three-dimensional (3-d) N based on an empirical relationship established computationally using the percolation model (see the SI, S2):

$$N = 0.93N_{2d}^{1.16}. \quad [4]$$

We determined the R_g of an aggregate from its pixelated SEM image by calculating the root mean square distance of all pixels (within the aggregate perimeter) from the aggregate geometric center. The θ_f of these particles was calculated with the knowledge of their N, a, and R_g using the equation:

$$\theta_f = N\left(a/R_g\right)^3. \quad [5]$$

Please note that we assumed in Equation (5) the R_g calculated from two-dimensional (2-d) microscope image to be equal to the true R_g of the aggregates in 3-d. Chakrabarty et al. (2011) showed in their simulation work the ratio of 2-d to 3-d R_g to be about 0.93 for DLCA aggregates in cluster-dilute regime. We show in the SI S3 that the ratio is about 0.98 for cluster-dense percolates.

We calculated the structure factor (S) of the sampled aggregates by performing Fourier transform on their projected images (Sorensen 2001; Heinson et al. 2017). Determination of S facilitated the double-checking for accuracy and consistency of D_f for these particles, per the scaling relationship that holds in the reciprocal-space (Sorensen 2001; Heinson et al. 2017):

$$S \propto \left(qR_g\right)^{-D_f}, \quad [6]$$

where q is the Fourier variable with the unit of inverse length. Please note that Equation (6) is only valid in the regime $1 < qR_g < R_g/a$ (Sorensen 2001; Heinson et al. 2017).

In another set of experiments, we dropped a total of 117 aggregates freshly produced from the ethylene BOF in the size-range 100 μm $< R_g <$ 1.5 mm in to stagnant air at 25°C and 1 atm. The M of these aggregates were estimated from their terminal settling velocity v_{ts} based

Table 1. Source of previously published data involved in our analysis and the experimental methods employed in this work

Experimental Sets		Generation Technique	Characterization Technique	Size Range R_g/a	Monomer Radius a (nm)
Cross et al. (2010)		Ethylene flat flame	DMA-CPMA-CPC	1-5	~16
This work	N1	DLCA model $f_v = 0.001$	N/A	2-400	Arbitrary
	N2	DLCA model $f_v = 0.003$	N/A	2-400	Arbitrary
	N3	DLCA model $f_v = 0.01$	N/A	2-300	Arbitrary
	N4	DLCA model $f_v = 0.02$	N/A	2-300	Arbitrary
	N5	DLCA model $f_v = 0.1$	N/A	2-200	Arbitrary
	N6	Percolation model	N/A	3-1,000	Arbitrary
	E1	Ethylene BOF	SEM image processing	30-5,000	~30
	E2	Ethylene BOF	Gravitational terminal settling and Stokes Law	3,000-50,000	~30

on the Stokes law (Friedlander 2000),

$$M = g^{-1} 6\pi\mu R_g \left[1 + 0.158\left(\frac{2\rho_f v_{ts} R_g}{\mu}\right)^{2/3}\right] v_{ts}, \quad [7]$$

where g is gravitational acceleration, μ and ρ_f are the air dynamic viscosity and density with the value of 1.8×10^{-5} Pa·s and 1.29 kg/m^3, respectively. Note that the measured v_{ts} was divided by a factor $C = 6.15 \pm 2.15$ prior to the calculation of M using Equation (7), per the work of Johnson et al. (1996). This precaution was taken to compensate for the systematic over-estimation of M when applying Stokes law on fractal aggregates that are porous and permeable (Johnson et al. 1996). The R_g of these aggregates were determined from their pixelated optical microscope images, according to the similar method discussed in previous paragraph. The θ_f of this set of aggregates was next determined using Equation (3).

We find it important to mention the assumption made when using Equations (3) and (5). The bulk volume of a fractal aggregate is approximated to be that of a sphere with radius R_g. The uncertainties that could stem from this assumption are investigated in detail in the Results section.

Numerical simulation

We performed two sets of numerical investigation to complement and theoretically validate our experimental findings. The first set of simulations involved generating 53,483 aggregates using the off-lattice DLCA algorithm (Meakin 1985, 1999). The detailed description of this algorithm can be found in references Heinson and Chakrabarty (2016), Heinson et al. (2017), and Heinson (2015). The initial monomer volume fraction (f_v), which is an important control parameter for aerosol aggregation, was varied between the extreme values of 0.001 and 0.1. The influence of f_v on the earliness of aerosol gelation was comprehensively discussed in reference Sorensen and Chakrabarti (2011). The second set of simulations involved using the percolation model to generate 10^4 aggregates (Stauffer and Aharony 1994; Heinson 2015). θ_f of all numerically generated aggregates were calculated using Equation (5). Table 1 summarizes the various experimental and numerical techniques employed in this study to generate and characterize particles in different size ranges for determination of their θ_f. The source of the mass-mobility data, based on which we inferred the θ_f for aggregates in the extremely small R_g/a limit, is also listed in Table 1.

Results and discussion

Spherical approximation of aggregate bulk volume

The uncertainty that stems from applying spherical geometry to approximate the bulk volume for aggregates, that is, $V_{\text{agg(sphere)}} = \frac{4}{3}\pi R_g^3$ is determined in this section. We do so by comparing $V_{\text{agg(sphere)}}$ to $V_{\text{agg(ellipsoid)}} = \frac{4}{3}\pi R_1 R_2 R_3$, where R_1, R_2, and R_3 are the three principal radii of an aggregate as well as an ellipsoid tightly bounding the aggregate. It has been shown that the use of these three principal radii takes into account the aggregate shape anisotropy (Heinson et al. 2010). In Figure 1, we plot the ratio $V_{\text{agg(sphere)}}/V_{\text{agg(ellipsoid)}}$ as a function of aggregate shape anisotropy$A = R_1/R_3$ for particles generated in experimental sets N1, N5, and N6. These three sets of particles represent cluster-dilute DLCA, cluster-dense DLCA, and percolates, respectively. One can see from Figure 1 that with increasing A, the ratio $V_{\text{agg(sphere)}}/V_{\text{agg(ellipsoid)}}$ increases monotonically for all particle sets. This trend implies that a spherical approximation leads to overestimation of the bulk volume of highly anisotropic aggregates with large A. However, had we used aggregate perimeter radius instead of its R_g, the ratio $V_{\text{agg(sphere)}}/$

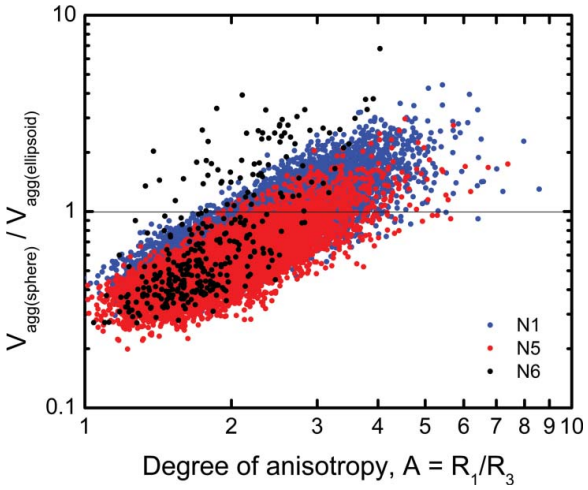

Figure 1. Ratio of $V_{agg(sphere)} = \frac{4}{3}\pi R_g^3$ to $V_{agg(ellipsoid)} = \frac{4}{3}\pi R_1 R_2 R_3$ as a function of shape anisotropy $A = R_1/R_3$ of the aggregates (or percolates) numerically generated using off-lattice DLCA model (sets N1 and N5) and percolation model (set N6).

$V_{agg(ellipsoid)}$ would always be greater than 1 for all aggregates. In other words, the use of R_g partially compensates for the overestimation stemming from the spherical volume approximation. For cluster-dilute DLCA aggregates, whose A distribution peaks at 2.5 (Heinson et al. 2010), the R_g-based spherical geometry reasonably approximates the aggregate bulk volume. We should also emphasize here that when DLCA aggregates gel, the shape of the resulting percolates tends to be more isotropic with smaller A. As A decreases, the percolate bulk volume would be underestimated, which would yield an overestimated θ_f. Finally, it is worth mentioning that the fractal scaling of θ_f would remain unaffected regardless of how the bulk volume of a particle is approximated. That is to say, the scaling exponent of θ_f would always be equal to $D_f - 3$ so long as an Euclidean object is chosen to represent the encompassing space.

Fractal scaling of θ_f

Figure 2 shows the comparison of the $\theta_f - R_g/a$ scaling relationships between aggregates studied by Cross et al. (2010) and that of sets N1–N6 from this study. Good agreement between Cross et al. (2010) and set N1 aggregates could be seen. Empirical fit to the data of set N1 aggregates following Equation (1) reveals an ensemble average $D_f = 1.80 \pm 0.01$, which is in good agreement with the prediction of DLCA growth mechanism in a cluster-dilute Brownian system (for example, $f_v = 0.001$). Comparison between sets N1 and N2 aggregates shows that for initial monomer $f_v = 0.003$, the decreasing trends of θ_f starts to deviate from the prediction of DLCA (black line) at $R_g/a =$ ca. 10^2. This inflection is an indication of the onset of aerosol gelation. Comparison between aggregates corresponding to sets N1–N5 shows that with an increase of initial monomer f_v, the inflection point shifts toward smaller R_g/a. This implies that gelation of DLCA aggregates takes place more readily in a denser (high f_v) sol system, which is in agreement with the prediction of aerosol-to-gel theory (Sorensen and Chakrabarti 2011). When an aggregating system starts out under extremely dense conditions, which correspond to $f_v = 0.1$ (set N5 aggregates), the scaling relationship of θ_f asymptotes to what the percolation model predicts (see the red line and set N6 data). Empirical fitting of the data corresponding to set N6 aggregates reveals a $D_f = 2.42 \pm 0.03$, which closely matches the $D_f \approx 2.5$ value observed for percolates. Summarizing Figure 2, we show the evolution of $\theta_f - R_g/a$ scaling relationships for aerosol aggregates in the small R_g/a limit.

Figure 3 shows the microscope images of the BOF-produced soot particles in the large R_g/a limit (corresponding to sets E1 and E2). We present this series of microscope images at changing degrees of magnification to give the readers a qualitative feel of the morphology of cluster-dense soot produced by our reactor. The constituent monomers, with a mean radius = 30 nm, are near spherical and point-contacting. At larger length scales, the monomers are no longer discernible; however, the fractal nature of the aggregates is still preserved, implying the scale-dependence of θ_f.

Figure 4 shows the comparison of $\theta_f - R_g/a$ scaling relationship for particles corresponding to sets N6, E1,

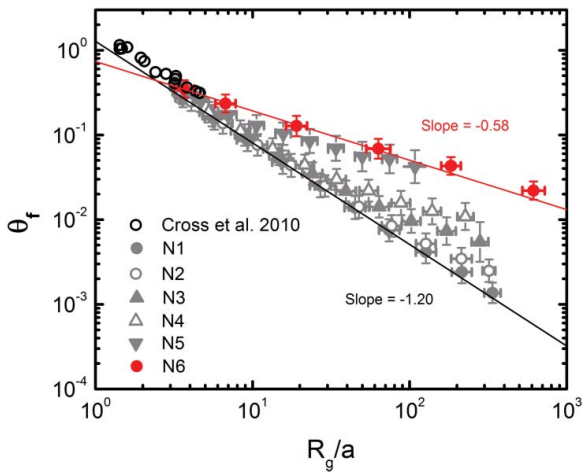

Figure 2. The $\theta_f - R_g/a$ scaling relationship of soot aggregates studied by Cross et al. (2010) compared to that of sets N1–N6 from this study. Error bars represent one geometric standard deviation. Least-square fitting of the data of sets N1 and N6 yields $\theta_f = 1.28 \pm 0.03 (R_g/a)^{-1.20 \pm 0.01}$ (lower [black] line) and $\theta_f = 0.74 \pm 0.08 (R_g/a)^{-0.58 \pm 0.06}$ (upper [red] line), respectively.

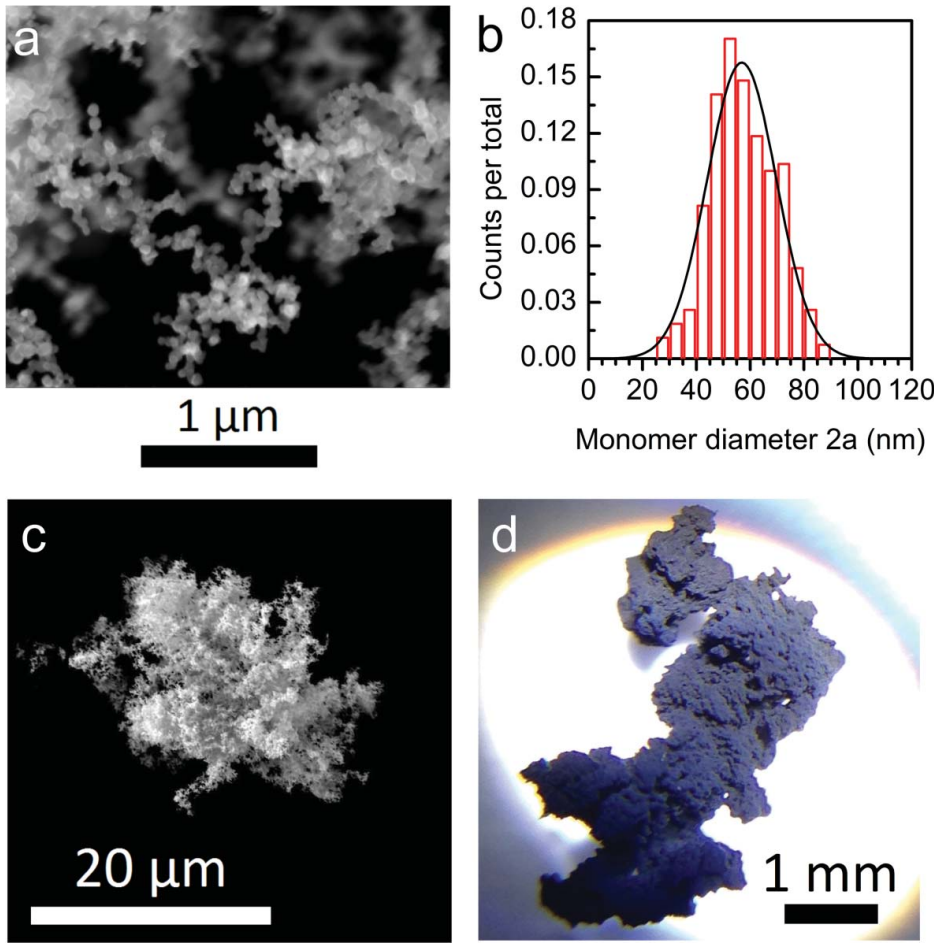

Figure 3. Morphologies of BOF produced soot (sets E1 and E2) at three different length scales. (a) SEM image showing the shape of the soot monomers. (b) The probability distribution of the monomer diameter 2*a*. Columns (red) represent the normalized counts of monomers within each size bin having a width of 5 nm. The solid line represents a Gaussian fit that peaks at 60.2 nm. (c) SEM image showing the soot morphology at micrometer scale. (d) Optical microscope image showing soot morphology at millimeter scale.

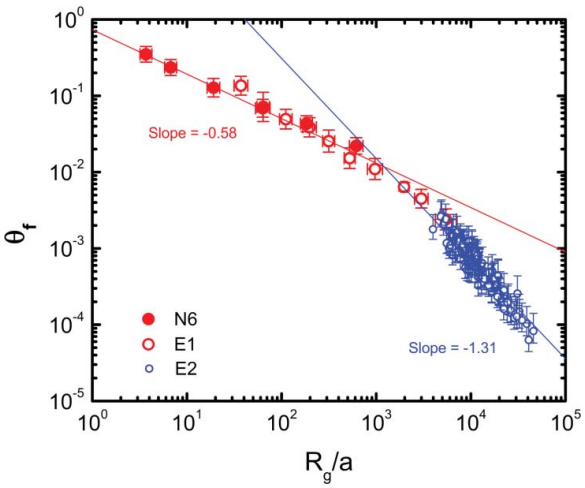

Figure 4. The $\theta_f - R_g/a$ scaling relationship of particles corresponding to sets N6, E1, and E2. Error bars represent one geometric standard deviation for N6 and E1 datasets. For the E2 dataset, errors stem from the uncertainty in $C = 6.15 \pm 2.15$ as reported by Johnson et al. (1996). Least-square fitting of the data of set E2 yields $\theta_f = 130.20 \pm 164.12\left(R_g/a\right)^{-1.31\pm0.14}$ (right-most [blue] line).

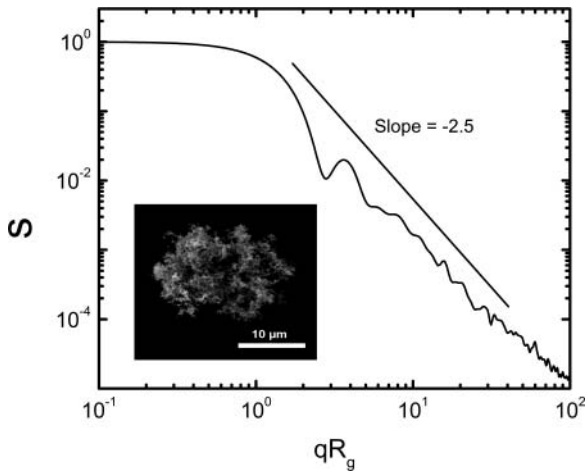

Figure 5. SEM image of a typical particle from set E1 and its structure factor in reciprocal space $S(qR_g)$. Black line with a slope $= -2.5$ serves as a guide to eyes.

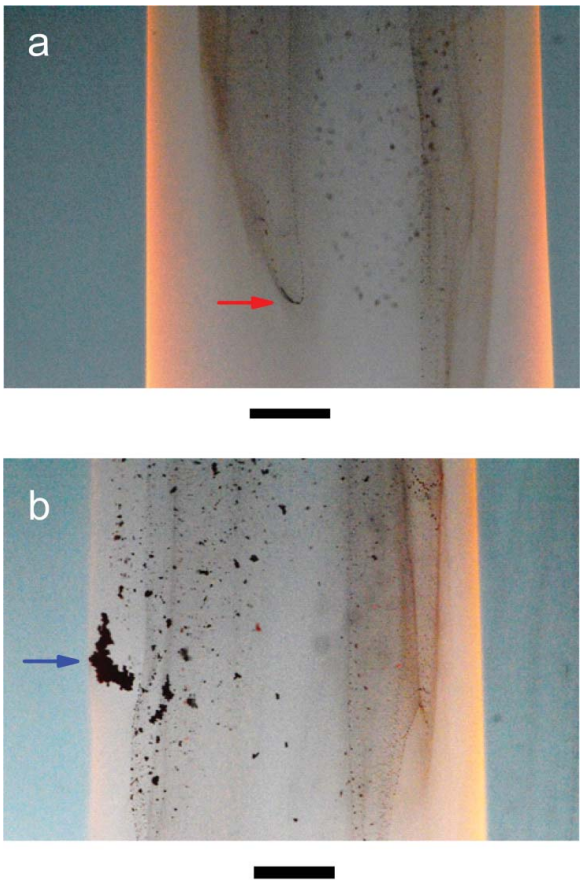

Figure 6. Photographs of the ethylene BOF. Scale bars are both 5 mm. Panel (a) shows a "dense-spot" location (indicated by the arrow) where sub-micron DLCA soot aggregates undergoes aerosol gelation. Panel (b) shows the spatial spreading out of percolates, who then participates in late-stage cluster-cluster aggregation as monomeric units. The resulting macro particle (or aggregated percolate) has a low D_f (the one marked by the arrow).

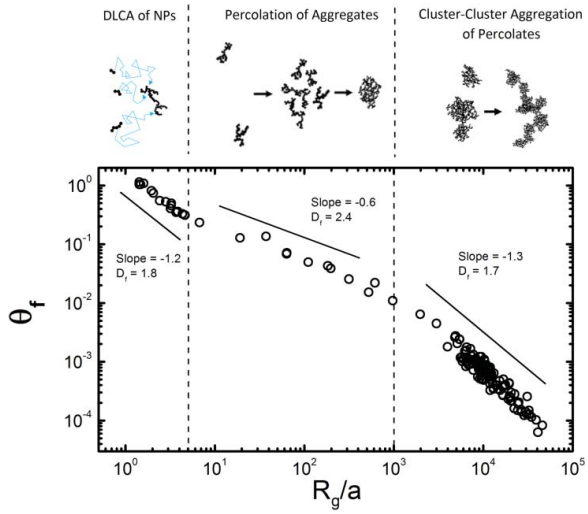

Figure 7. Generalized picture of the scale dependence of θ_f for soot aggregates. With R_g/a increasing from 1 to 5×10^4, three successive growth regimes were identified, namely, diffusion-limited cluster-cluster aggregation (DLCA) of nanoparticles (NPs; also referred to as monomers), percolation of aggregates, and cluster-cluster aggregation of percolates. These growth mechanisms are sketched on top of the figure with their corresponding cross-over points at $R_g/a = 5$ and 10^3. Note that these cross-over R_g/a could be highly system dependent. Blacklines with slopes $= -1.2$, -0.4, and -1.3 serve as guide to eyes.

and E2. The E1 dataset, obtained from digital processing of SEM images of BOF-generated soot, deviates slightly from the prediction of the percolation model (red dash line). This slight deviation may arise from the artifacts associated with the particle sampling process. Inertial impaction could cause deformation of an aggregate's silhouette (or outer structure) but not its internal structure and monomer packing arrangements. This is evident from the structure factor $S(qR_g)$ plot in Figure 5, which contains details on a particle's internal structure. Beyond the Guinier regime ($qR_g > 1$), S is observed to scale with ${qR_g}^{-2.5}$ in concurrence with the D_f of percolates.

Particles corresponding to sets E1 and E2 have R_g/a in the large limit, that is, $\geq 10^3$. The power-law exponent of θ_f versus R_g/a for these particles gradually decreases to a new value of -1.31 ± 0.14 (blue dash line). Per Equation (1), this exponent suggests a distinct $D_f \approx 1.7$, which implies a growth mechanism involving the cluster-cluster aggregation of individual percolates. Visually, we are encountering a scenario where for $R_g/a > 10^3$ the volume spanning percolates start to act like monomers and participate in a late-stage cluster-cluster aggregation process. The dynamics of this late-stage aggregation, which is beyond the typical length-scale of aerosol gelation (Kim et al. 2006; Sorensen and Chakrabarti 2011), has yet to be systematically studied in flame systems.

We make an attempt to provide a phenomenological understanding of the occurrence of this late-stage aggregation of percolates, which is observed experimentally but not captured theoretically in our simulations. Aggregation in open-flow systems, such as flames, deviates from the idealized systems described in the aerosol-to-gel transition theory (Sorensen and Chakrabarti 2011). The spatial distribution of particle f_v could be largely inhomogenous in flames. This gives rise to "dense-spots" in which the f_v of particles is substantially higher than the surroundings, and percolates with $D_f \approx 2.5$ are readily formed. For example, Figure 6a shows a "dense-spot" in the body of our BOF. The sub-volume wherein the recirculating particle-laden gas flow makes a "U-turn" becomes densely populated with DLCA aggregates (see the location indicated by the red arrow in panel (a)). At this dense-spot, the aerosol-to-gel transition is so prominent that it is visible to naked eyes. Next, the

individual percolates formed in these dense-spots are observed to be spatially spreading out (see Figure 6b). These diverging percolates, whose average nearest neighbor separation distance is much larger than their average size, eventually start to behave as monomeric units leading to collision with each other before irreversibly forming the millimeter-size, chain-like, and open-structure aggregates demonstrating a low D_f of ≈1.7 (see the particle indicated by the blue arrow in panel (b)). A qualitative explanation for why the D_f of these particles appears to be smaller than the typical value of 1.8–1.9 expected for a 3-d cluster-cluster aggregation mechanism is briefly provided here. *In situ* tracking of particle motion in our flame system reveals that the particle trajectories are tightly bound in a 3-d annular region close to the flame front (please refer to the figure in the SI S4). The thickness of this annular is about 5 mm, which is slightly larger than the mean size of these particles. This confined geometry limits the collisions between a pair of particles to be quasi 3-d in nature, meaning that the probability of particle–particle collision along the radial direction (see Figure S4) is comparatively lower than along the angular and vertical directions. We infer that this constrained collisional arrangement may have led to a D_f slightly smaller in value than that resulting from unconstrained 3-d cluster-cluster aggregation. On the other hand, this value is still much greater than $D_f \approx 1.4$ resulting from a 2-d cluster-cluster aggregation growth mechanism (Sorensen and Hageman 2001).

Conclusion

We now stitch together and summarize the results from above, and draw a picture of the scaling variance for θ_f as a function of R_g/a across five orders of magnitude length scale (Figure 7). θ_f decreases in distinct power-law exponents of -1.20 ± 0.01, -0.58 ± 0.06, and -1.31 ± 0.14 successively. Fractal nature of soot aggregates is shown to hold even as R_g/a reaches the extremely large limit of 5×10^4. The θ_f – R_g/a scaling power-law exponents reveal three successive aggregate growth regimes, namely, DLCA of monomers, percolation of aggregates, and cluster-cluster aggregation of percolates. The late-stage recurrence of cluster-cluster aggregation in the large R_g/a limit, ca. $\geq 10^3$, could be system dependent and needs to be verified for other sol systems (Sorensen and Feke 1996; Sorensen and Hageman 2001; Kim et al. 2006). Our observation of this fractal scale dependence of θ_f in the large R_g/a limit has important implications for the synthesis of materials with tunable porosity, extremely low density and refractive index, and high surface area per unit volume (Johnson et al. 1996; Sánchez-González et al. 2005; Dhaubhadel et al. 2007; Greaves et al. 2011; Chakrabarty et al. 2014b; Liu et al. 2015; Sakai et al. 2016) and accurate estimation of radiative forcing by carbonaceous aerosols (Bond et al. 2013; Chakrabarty et al. 2014a; Heinson and Chakrabarty 2016).

Acknowledgments

The authors thank Dr. Christopher M. Sorensen at Kansas State University and Dr. Richard L. Axelbaum at Washington University in St. Louis for valuable discussions on this work. The authors also thank Mike K. Shen and Akshay Gopan for their assistance with flame photographing.

Funding

This work was supported by the US National Science Foundation (NSF) grants AGS-1455215 and CBET-1511964, and the NASA Radiation Sciences Program grant NNX15AI66G.

References

Bond, T. C., Doherty, S. J., Fahey, D. W., Forster, P. M., Berntsen, T., DeAngelo, B. J., Flanner, M. G., Gan, S., Kärcher, B., Koch, D., Kinne, S., Kondo, Y., Quinn, P. K., Sarofim, M. C., Schultz, M. G., Schulz, M., Venkataraman, C., Zhang, H., Zhang, S., Bellouin, N., Guttikunda, S. K., Hopke, P. K., Jacobson, M. Z., Kaiser, J. W., Klimont, Z., Lohmann, U., Schwarz, J. P., Shindell, D., Storelvmo, T., Warren, S. G., and Zender, C. S. (2013). Bounding the Role of Black Carbon in the Climate System: A Scientific Assessment. *J. Geophys. Res.*, 118:5380–5552.

Chakrabarty, R. K., Beres, N. D., Moosmüller, H., China, S., Mazzoleni, C., Dubey, M. K., Liu, L., and Mishchenko, M. I. (2014a). Soot Superaggregates from Flaming Wildfires and Their Direct Radiative Forcing. *Sci. Rep.*, 4:5508.

Chakrabarty, R. K., Garro, M. A., Garro, B. A., Chancellor, S., Moosmüller, H., and Herald, C. M. (2011). Simulation of Aggregates with Point-Contacting Monomers in the Cluster–Dilute Regime. Part 2: Comparison of Two-and Three-Dimensional Structural Properties as a Function of Fractal Dimension. *Aerosol Sci. Technol.*, 45:903–908.

Chakrabarty, R. K., Moosmüller, H., Garro, M. A., and Stipe, C. B. (2012). Observation of Superaggregates from a Reversed Gravity Low-Sooting Flame. *Aerosol Sci. Technol.*, 46:i–iii.

Chakrabarty, R. K., Novosselov, I. V., Beres, N. D., Moosmüller, H., Sorensen, C. M., and Stipe, C. B. (2014b). Trapping and Aerogelation of Nanoparticles in Negative Gravity Hydrocarbon Flames. *Appl. Phys. Lett.*, 104:243103.

Chao, B. H., Liu, S., and Axelbaum, R. L. (1998). On Soot Inception in Nonpremixed Flames and the Effects of Flame Structure. *Combust. Sci. Technol.*, 138:105–135.

Cross, E. S., Onasch, T. B., Ahern, A., Wrobel, W., Slowik, J. G., Olfert, J., Lack, D. A., Massoli, P., Cappa, C. D., Schwarz, J. P., Spackman, J. R., Fahey, D. W., Sedlacek, A., Trimborn, A., Jayne, J. T., Freedman, A., Williams, L. R., Ng, N. L., Mazzoleni, C., Dubey, M., Brem, B., Kok, G., Subramanian,

R., Freitag, S., Clarke, A., Thornhill, D., Marr, L. C., Kolb, C. E., Worsnop, D. R., and Davidovits, P. (2010). Soot Particle Studies—Instrument Inter-Comparison—Project Overview. *Aerosol Sci. Technol.*, 44:592–611.

Dhaubhadel, R., Gerving, C. S., Chakrabarti, A., and Sorensen, C. M. (2007). Aerosol Gelation: Synthesis of a Novel, Lightweight, High Specific Surface Area Material. *Aerosol Sci. Technol.*, 41:804–810.

Forrest, S. R., and Witten Jr, T. A. (1979). Long-Range Correlations in Smoke-Particle Aggregates. *J. Phys. A*, 12:L109–L117.

Friedlander, S. K. (2000). *Smoke, Dust and Haze: Fundamental of Aerosol Dynamics*. Oxford University Press, New York, pp. 109.

Greaves, G. N., Greer, A. L., Lakes, R. S., and Rouxel, T. (2011). Poisson's Ratio and Modern Materials. *Nat. Mater.*, 10:823–837.

Heinson, W. R. (2015). *Simulation Studies on Shape and Growth Kinetics for Fractal Aggregates in Aerosol and Colloidal Systems*. Ph.D. Thesis, Kansas State University.

Heinson, W. R., and Chakrabarty, R. K. (2016). Fractal Morphology of Black Carbon Aerosol Enhances Absorption in the Thermal Infrared Wavelengths. *Opt. Lett.*, 41:808–811.

Heinson, W. R., Liu, P., and Chakrabarty, R. K. (2017). Fractal Scaling of Coated Soot Aggregates. *Aerosol Sci. Technol.*, 51:12–19.

Heinson, W. R., Sorensen, C. M., and Chakrabarti, A. (2010). Does Shape Anisotropy Control the Fractal Dimension in Diffusion-Limited Cluster-Cluster Aggregation? *Aerosol Sci. Technol.*, 44:i–iv.

Hinds, W. C. (1999). *Aerosol Technology: Properties, Behavior, and Measurement of Airborne Particles*. Wiley, New York, pp. 233–249.

Johnson, C. P., Li, X., and Logan, B. E. (1996). Settling Velocities of Fractal Aggregates. *Environ. Sci. Technol.*, 30:1911–1918.

Kim, W., Sorensen, C. M., Fry, D., and Chakrabarti, A. (2006). Soot Aggregates, Superaggregates and Gel-Like Networks in Laminar Diffusion Flames. *J. Aerosol Sci.*, 37:386–401.

Kumfer, B. M., Skeen, S. A., Chen, R., and Axelbaum, R. L. (2006). Measurement and Analysis of Soot Inception Limits of Oxygen-Enriched Coflow Flames. *Combust. Flame*, 147:233–242.

Law, C. K. (2010). *Combustion Physics*. Cambridge University Press, New York, pp. 119–121.

Liu, P., Arnold, I. J., Wang, Y., Yu, Y., Fang, J., Biswas, P., and Chakrabarty, R. K. (2015). Synthesis of Titanium Dioxide Aerosol Gels in a Buoyancy-Opposed Flame Reactor. *Aerosol Sci. Technol.*, 49:1232–1241.

Liu, P., and Chakrabarty, R. K. (2016). Sensitivity Analysis of Aggregate Morphology on Mass-Mobility Relationship and Improved Parameterizations. *Aerosol Sci. Technol.*, 50:63–70.

Manley, S., Cipelletti, L., Trappe, V., Bailey, A. E., Christianson, R. J., Gasser, U., Prasad, V., Segre, P. N., Doherty, M. P., Sankaran, S., Jankovsky, A. L., Shiley, B., Bowen, J., Eggers, J., Kurta, J., Kurta, C., Lorik, T., and Weitz, D. A. (2004). Limits to Gelation in Colloidal Aggregation. *Phys. Rev. Lett.*, 93:108302.

Meakin, P. (1985). Off Lattice Simulations of Cluster-Cluster Aggregation in Dimensions 2–6. *Phys. Lett. A*, 107:269–272.

Meakin, P. (1999). A Historical Introduction to Computer Models for Fractal Aggregates. *J. Sol-Gel Sci. Technol.*, 15:97–117.

Park, K., Kittelson, D. B., and McMurry, P. H. (2004). Structural Properties of Diesel Exhaust Particles Measured by Transmission Electron Microscopy (TEM): Relationships to Particle Mass and Mobility. *Aerosol Sci. Technol.*, 38:881–889.

Rehman, I. H., Ahmed, T., Praveen, P. S., Kar, A., and Ramanathan, V. (2011). Black Carbon Emissions from Biomass and Fossil Fuels in Rural India. *Atmos. Chem. Phys.*, 11:7289–7299.

Sakai, K., Kobayashi, Y., Saito, T., and Isogai, A. (2016). Partitioned Airs at Microscale and Nanoscale: Thermal Diffusivity in Ultrahigh Porosity Solids of Nanocellulose. *Sci. Rep.*, 6:20434.

Sánchez-González, J., Macías-García, A., Alexandre-Franco, M. F., and Gómez-Serrano, V. (2005). Electrical Conductivity of Carbon Backs under Compression. *Carbon*, 43:741–747.

Sorensen, C. M. (2001). Light Scattering by Fractal Aggregates: A Review. *Aerosol Sci. Technol.*, 35:648–687.

Sorensen, C. M. (2011). The Mobility of Fractal Aggregates: A Review. *Aerosol Sci. Technol.*, 45:765–779.

Sorensen, C. M., and Chakrabarti, A. (2011). The Sol to Gel Transition in Irreversible Particulate Systems. *Soft Matter*, 7:2284–2296.

Sorensen, C. M., and Feke, G. D. (1996). The Morphology of Macroscopic Soot. *Aerosol Sci. Technol.*, 25:328–337.

Sorensen, C. M., and Hageman, W. B. (2001). Two-Dimensional Soot. *Langmuir*, 17:5431–5434.

Sorensen, C. M., Hageman, W. B., Rush, T. J., Huang, H., and Oh, C. (1998). Aerogelation in a Flame Soot Aerosol. *Phys. Rev. Lett.*, 80:1782–1785.

Stauffer, D., and Aharony, A. (1994). *Introduction to Percolation Theory*. Taylor and Francis, London, pp. 153–168.

Taulbee, D. B., and Yu, C. P. (1975). A Theory of Aerosol Deposition in the Human Respiratory Tract. *J. Appl. Physiol.*, 38:77–85.

Zangmeister, C. D., Radney, J. G., Dockery, L. T., Young, J. T., Ma, X., You, R., and Zachariah, M. R. (2014). Packing Density of Rigid Aggregates is Independent of Scale. *Proc. Natl. Acad. Sci. U.S.A.*, 111:9037–9041.